

Article

Chromophoric Dissolved Organic Matter and Dissolved Organic Carbon from Sea-Viewing Wide Field-of-View Sensor (SeaWiFS), Moderate Resolution Imaging Spectroradiometer (MODIS) and MERIS Sensors: Case Study for the Northern Gulf of Mexico

Nazanin Chaichi Tehrani ¹, Eurico J. D'Sa ^{1,*}, Christopher L. Osburn ², Thomas S. Bianchi ³ and Blake A. Schaeffer ⁴

¹ Department of Oceanography and Coastal Sciences, Louisiana State University, Baton Rouge, LA 70803, USA; E-Mail: nchaichi@gmail.com

² Department of Marine, Earth and Atmospheric Science, North Carolina State University, Raleigh, NC 27695, USA; E-Mail: closburn@ncsu.edu

³ Department of Oceanography, Texas A&M University, College Station, TX 77843, USA; E-Mail: tbianchi@geos.tamu.edu

⁴ US EPA Gulf Ecology Division, Gulf Breeze, FL 32561, USA; E-Mail: schaeffer.blake@epamail.epa.gov

* Author to whom correspondence should be addressed; E-Mail: ejdsa@lsu.edu; Tel.: +1-225-578-0212.

Received: 4 January 2013; in revised form: 6 March 2013 / Accepted: 12 March 2013 /

Published: 19 March 2013

Abstract: Empirical band ratio algorithms for the estimation of colored dissolved organic matter (CDOM) and dissolved organic carbon (DOC) for Sea-viewing Wide Field-of-view Sensor (SeaWiFS), Moderate Resolution Imaging Spectroradiometer (MODIS) and MERIS ocean color sensors were assessed and developed for the northern Gulf of Mexico. Match-ups between *in situ* measurements of CDOM absorption coefficients at 412 nm ($a_{\text{CDOM}(412)}$) with that derived from SeaWiFS were examined using two previously reported reflectance band ratio algorithms. Results indicate better performance using the $R_{\text{rs}}(510)/R_{\text{rs}}(555)$ (Bias = -0.045 ; RMSE = 0.23; SI = 0.49, and $R^2 = 0.66$) than the $R_{\text{rs}}(490)/R_{\text{rs}}(555)$ reflectance band ratio algorithm. Further, a comparison of $a_{\text{CDOM}(412)}$ retrievals using the $R_{\text{rs}}(488)/R_{\text{rs}}(555)$ for MODIS and $R_{\text{rs}}(510)/R_{\text{rs}}(560)$ for MERIS reflectance band ratios revealed better CDOM retrievals with MERIS data. Since DOC

cannot be measured directly by remote sensors, CDOM as the colored component of DOC is utilized as a proxy to estimate DOC remotely. A seasonal relationship between CDOM and DOC was established for the summer and spring-winter with high correlation for both periods ($R^2 \sim 0.9$). Seasonal band ratio empirical algorithms to estimate DOC were thus developed using the relationships between CDOM- R_{rs} and seasonal CDOM-DOC for SeaWiFS, MODIS and MERIS. Results of match-up comparisons revealed DOC estimates by both MODIS and MERIS to be relatively more accurate during summer time, while both of them underestimated DOC during spring-winter time. A better DOC estimate from MERIS in comparison to MODIS in spring-winter could be attributed to its similarity with the SeaWiFS band ratio CDOM algorithm.

Keyword: CDOM; DOC; SeaWiFS; MODIS; MERIS

1. Introduction

Dissolved organic matter (DOM), the largest bioreactive inventory of carbon in the global ocean comparable in size to the atmospheric CO₂ stock has a major impact on the global carbon cycle and climate change [1,2]. The abundance of DOM has generally been determined as dissolved organic carbon (DOC), a major component of organic carbon [3]. Chromophoric DOM (CDOM), the colored component of DOM primarily absorbs light in the UV and visible spectral range affecting the intensity and spectral quality of the light field in the aquatic medium. Because *in situ* measurement and analysis of DOC is time-consuming and expensive [4,5], the potential for satellite estimates of DOC could provide a useful tool with synoptic and repeated coverage. However, DOC cannot be sensed directly by ocean color sensors; CDOM, the colored fraction of DOC, can be estimated remotely. Thus, CDOM can be utilized as an inexpensive intermediary to estimate the standing stock of DOC and the carbon cycle in aquatic environments. Coble [6] reported CDOM's contribution to DOC ranged from 20% to 70% in the ocean. The optical signature of CDOM can thus be used as a proxy for DOC as long as these two parameters behave conservatively in the marine environment [7,8]. However, a robust bio-optical algorithm to retrieve CDOM from ocean color sensors must be available [7].

CDOM as well as other photoreactive in-water constituents (e.g., chlorophyll-a, detritus or non-algal particles) affect the underwater light field and the optical properties of water [9,10]. Hence, several ocean color algorithms have been developed to study CDOM distribution both spatially and temporally. Semi-analytical (SA) inversion models have been developed for the Sea-viewing Wide Field-of-view Sensor (SeaWiFS) and Moderate Resolution Imaging Spectroradiometer (MODIS) to derive CDOM and detritus absorption coefficient as a single component (CDM) [11–14], as both exhibit similar spectral shape and slope in the visible light spectrum [15]. In order to investigate carbon cycling in coastal and estuarine waters (Case-2 waters) where optically active constituents often do not co-vary with chlorophyll-a, knowledge of CDOM's distribution and dynamics is required [16–18]. Empirical algorithms, also known as band ratio algorithms, are based on statistical relationships between R_{rs} band ratios and the concentration of seawater constituents [18–23]. For example, Kahru and Mitchell [19] developed a relationship between $a_{CDOM}(300)$ and SeaWiFS

$R_{rs}(443)/R_{rs}(510)$ at the CalCOFI site in southern California. D'Sa and Miller [20] developed an algorithm to retrieve $a_{CDOM}(412)$ from ocean color data in the Mississippi River dominated coastal waters using a relationship between $a_{CDOM}(412)$ and the SeaWiFS reflectance band ratio of $R_{rs}(510)/R_{rs}(555)$. For the coastal waters adjacent to the Chesapeake and Delaware Bays, Johannessen *et al.* [21] reported the relationship between ultraviolet (UV) attenuation coefficient (K_d) at 323 nm, 338 nm, and 380 nm and the $R_{rs}(412)/R_{rs}(555)$ band ratio. Recently, Zhu *et al.* [24] developed an Extended Quasi-Analytical Algorithm (QAA-E) to estimate CDOM in the Mississippi and Atchafalaya River plume regions using above-surface hyper-spectral light measurements.

Conservative behavior between CDOM absorption coefficient and DOC has been reported in different types of water bodies [8,25–28]. CDOM absorption coefficient ($a_{CDOM}(\lambda)$) and DOC concentration are highly correlated with each other in regions where the mixing of fresh and oceanic waters control the variability of each parameter and terrestrial dominance is strong [29]. These conditions have enabled satellite estimates of DOC using the relationship between CDOM-DOC and CDOM- R_{rs} band ratios [7,22]. Mannino *et al.* [22] developed algorithms to derive DOC through the relationship between the a_{CDOM} at 412 nm, 355 nm, DOC, and R_{rs} ratios for MODIS/Aqua and SeaWiFS in coastal waters of the US Middle Atlantic Bight. Del Castillo and Miller [7] applied the $R_{rs}(510)/R_{rs}(670)$ band ratio to SeaWiFS imagery to retrieve DOC in the Mississippi River plume. The high rates of water discharge containing elevated levels of DOC and CDOM by the Mississippi and Atchafalaya Rivers into the coastal waters strongly impacts the biogeochemical processes and fluxes in the northern Gulf of Mexico. Satellite ocean color remote sensing offers the capability to monitor CDOM and DOC distribution spatially and temporally and to improve understanding of the carbon cycling in this large river delta-front estuary (LDE) [30].

The primary goal of this study is to evaluate existing and to develop new ocean color algorithms for CDOM absorption and DOC concentrations in the northern Gulf of Mexico. An extended set of field CDOM absorption and DOC measurements collated for the northern Gulf of Mexico as part of a NASA funded project were used in this study. Algorithm assessment and development were based on two empirical band ratio CDOM algorithms, namely the D'Sa *et al.* [18] and the Mannino *et al.* [22] algorithms for estimating $a_{CDOM}(412)$. These algorithms were extended to MODIS/Aqua and the MERIS/ENVISAT sensors. Further, DOC empirical algorithms were developed through the relationships between *in situ* $a_{CDOM}(412)$ -*in situ* DOC and *in situ* $a_{CDOM}(412)$ - R_{rs} band ratios (satellite-derived) (e.g., Mannino *et al.* [22]). This approach was found to be an effective method to derive DOC concentration. The satellite-derived DOC concentration enabled us to monitor DOC variations both spatially and temporally, and to enhance our understanding of the organic carbon processes in this LDE in the northern Gulf of Mexico.

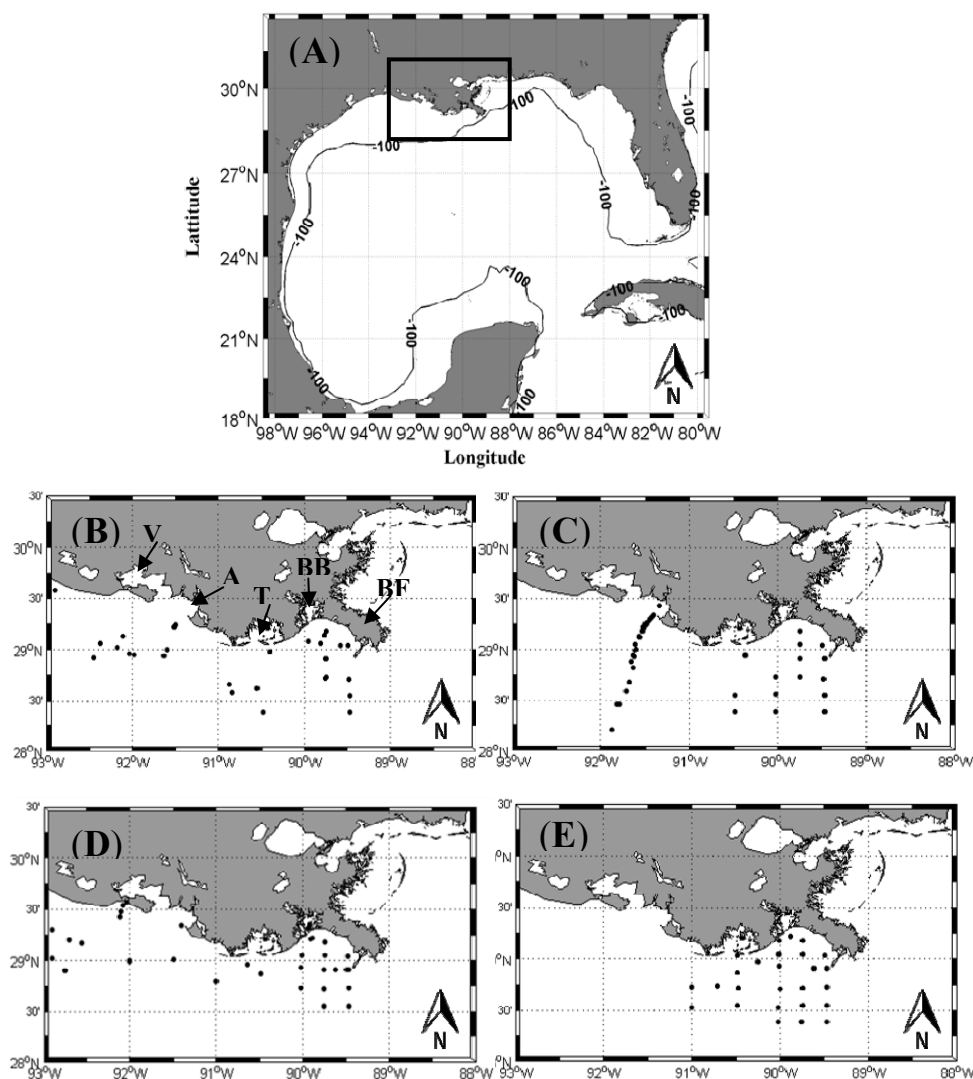
2. Materials and Methods

2.1. Study Area

The study area is located in the northern Gulf of Mexico on the Texas-Louisiana shelf, covering the region from latitude 28.0° to 30.5°N and longitude 88.0° to 93.0°W (Figure 1(A)). The study site is highly influenced by the discharge from the Mississippi River (MR) and its largest tributary, the Atchafalaya River (AR). The Mississippi River drains approximately 41% of the contiguous United

States, making it the third largest drainage basin in the world. The MR also ranks as the seventh largest river in terms of fresh water discharge [31,32]. The Mississippi-Atchafalaya River System (MARS) discharges ~70% of its total flow into the Gulf of Mexico through the MR Birdfoot delta while the remainder discharges through the AR and Wax Lake outlets into the broad, shallow Atchafalaya bay [33,34]. Seasonal variations and the large discharge of freshwater from the MR and AR profoundly influence the bio-optical properties of water, primary productivity, and the distribution of carbon flux in the region [20,34–37]. Terrestrially-derived (riverine or allochthonous) CDOM introduced by the MR and AR predominates the northern Gulf of Mexico [38]. The annual export of DOC from the Mississippi and the Atchafalaya Rivers into the Gulf of Mexico was reported 1.75 Tg and 0.95 Tg, respectively. These amounts account for about 0.8%–1.1% of the total global input of DOC from rivers to the ocean [39].

Figure 1. (A) Map of the study area in the northern Gulf of Mexico. Location of stations in; (B) March, May, July and August 2005; (C) March, April, May, July 2007; (D) February, April, June 2008, (E) August 2009. BFD, BB, TB, AB and VB indicate birdfoot Delta, Barataria Bay, Terrebonne Bay, Atchafalaya Bay and Vermilion Bay, respectively.



2.2. Field Sampling

Field data comprising of CDOM optical (spectral absorption coefficient) and DOC concentrations in conjunction with physical (salinity) properties of water were obtained from the study area during 17 oceanographic cruises in 2005 and 2007–2009 (Table 1; Figure 1). Some of the field data from these cruises were hosted as part of a NASA funded project by the Biological and Chemical Oceanography Data Management Office (BCO-DMO) as a data rescue effort. In the spring and summer (March, May, July, and August) of 2005, coastal waters influenced by the MR from Southwest Pass to the Atchafalaya Delta were sampled aboard the *RV Gyre*. Water samples were collected from the surface using Niskin bottles attached to the conductivity-temperature-depth (CTD) profiler (Sea-Bird Electronic, Inc., Bellevue, WA, USA). The samples were filtered through pre-rinsed 0.2 μm Nuclepore membrane filters within three hours of collection. Spectral absorption of filtered samples was obtained onboard the ship using a single-beam spectrophotometer [40]. Water samples taken in April 2007 were collected and analyzed similar to the samples taken in 2005. Field samples collected in May 2007 in the AR plume region onboard *RV Pelican* were obtained from the Biological and Chemical Oceanography Data Management Office (BCO-DMO) website (http://data.bco-dmo.org/jg/serv/BCO/NACP_Coastal/GulfMexico), samples were filtered through 0.2 μm Polyether sulfone filters into baked (550 °C; 5 h minimum) collection vials and stored at 4 °C in the dark until processed in the laboratory. More information can be found on the BCO-DMO website.

Table 1. Field data from cruises in the northern Gulf of Mexico along with mean values for $a_{\text{CDOM}(412)}$, dissolved organic carbon (DOC) concentration, salinity, and S.D., and Geometric mean for each cruise.

Cruise	Date	$a_{\text{CDOM}(412)}$ (m^{-1})	DOC ($\mu\text{mol}\cdot\text{C}\cdot\text{L}^{-1}$)	Salinity (psu)	S.D. $a_{\text{CDOM}(412)}$	Geometric Mean $a_{\text{CDOM}(412)}$
1	23–29 March 2005	0.47	n/a	27.07	0.22	0.43
2	20–25 May 2005	0.43	n/a	27.07	0.16	0.39
3	8–12 July 2005	0.23	n/a	29.27	0.18	0.17
4	18–24 August 2005	0.25	n/a	28.75	0.13	0.22
5	23–28 March 2007	n/a	204.51	n/a	-	-
6	16–20 April 2007	2.79	n/a	31.75	2.09	1.62
7	7–10 May 2007	0.87	180.02	24.16	0.93	0.33
8	17 and 19 July 2007	1.43	288.23	15.12	0.60	1.34
9	17–20 July 2007	n/a	155.13	n/a	-	-
10	9 August 2007	0.74	266.58	27.64	0.20	0.73
11	11 and 13 September 2007	1.97	509.74	11.33	0.44	1.93
12	9–12 February 2008	1.72	361.68	11.28	0.58	1.64
13	5–8 April 2008	3.72	664.30	2.60	1.35	3.49
14	6–8 April 2008	0.82	n/a	22.33	0.56	0.55
15	6–18 April 2008	n/a	226.69	n/a	-	-
16	2 June 2008	2.52	377.25	11.23	0.19	2.51
17	18–20 August 2009	0.34	166.97	27.94	0.27	0.22

In situ data obtained during the 2007 (July, August, September) and 2008 (February, April, June) cruises were also used. Near-shore sampling was conducted from a small boat in transects out of the

Vermilion, Atchafalaya, Terrebonne, and Barataria Bays, and the Mississippi River's Southwest Pass. Discrete water samples were collected 0.5 m below the water surface using a Sea-Bird 25 CTD. Water samples were filtered through Whatman 47 mm GF/F filters, nominal pore size 0.7 μm , into combusted glass flasks for CDOM and DOC analysis [41]. DOC measurements were obtained during cruises onboard the *RV Pelican* in March and July of 2007 and April and July of 2008 as part of the Mechanisms Controlling Hypoxia (MCH) project. In August 2009, *in situ* observations were made onboard the *RV Pelican* on the Louisiana continental shelf. *In situ* samples from the water surface were collected using Niskin bottles attached to CTD profiles. Samples were immediately filtered under low vacuum through a Whatman GF/F filter (nominal pore size 0.2 μm) and then stored in pre-cleaned amber glass bottles and refrigerated until CDOM absorption and DOC concentration were measured in the laboratory.

2.3. CDOM Absorption

Spectral CDOM absorption values from filtered water obtained in 2005 were determined onboard the ship using a capillary waveguide system (WPI, Inc., Sarasota, FL, USA), a single-beam spectrophotometer [42,43]. The optical absorbance spectra (A) were obtained between 250 nm to 722 nm from two scans, namely, a cell filled with blank solution (Milli-Q water), adjusted for the sample salinity followed by a water sample scan. The absorbance values at each wavelength were corrected for baseline fluctuation and scattering by subtracting the absorbance averaged between 715 to 722 nm [40]. The absorption coefficients at each wavelength ($a_{\text{CDOM}}(\lambda)$) (m^{-1}) were calculated using the following equation:

$$a(\lambda) = \frac{2.303 A(\lambda)}{l} \quad (1)$$

where l , the optical path length (m) used for the absorbance measurements were 0.1 or 0.5 m [40].

CDOM absorption from filtered water samples obtained during 2007 (July, August, September) and 2008 (February, April, June) were obtained with a Shimadzu UV1700 dual-beam spectrophotometer using a 1-cm cuvette at 1 nm intervals between 350–700 nm. Spectra were then normalized by subtracting each wavelength from the measured value at 700 nm [41]. The CDOM absorption measurement method used to analyze the May 2007 water samples is documented at BCO-DMO website (http://data.bco-dmo.org/jg/serv/BCO/NACP_Coastal/GulfMexico/CDOM.html0). Filtered samples from the August 2009 survey were processed in the laboratory on a double beam Perkin Elmer Lambda 850 spectrophotometer between 190 to 750 nm at 2 nm intervals. Samples were brought to room temperature before measuring the absorbance spectra of CDOM. Before determining $a_{\text{CDOM}}(\lambda)$, absorbance data were corrected by subtracting the mean absorbance from 700 to 750 nm from each wavelength. The CDOM absorption coefficient at each wavelength was derived using Equation (1).

2.4. DOC Concentration

The DOC concentration of filtered-water samples obtained in 2007 (July, August, September) and in 2008 (February, April, June) was measured using a Shimadzu TOC–VCSN analyzer, calibrated with potassium biphthalate [41]. Samples collected in 2007 (March, July) and 2008 (April, July) were

filtered through GF/F filters and then acidified (100 μ L of 2 N HCl was added in order to remove inorganic carbon). The DOC concentration was then measured with the Shimadzu TOC-VCSH/CSN by using high-temperature catalytic oxidation (HTCO). The DOC concentrations used for this study from the May 2007 cruise were measured by wet chemical oxidation with an OI Analytical Model 1010 TOC analyzer [44]. For the August 2009 samples, DOC concentrations were obtained using a Shimadzu TOC-5000A (with ASI-5000A auto-sampler) using a high temperature combustion method.

2.5. Satellite Data

Satellite data from the SeaWiFS, MODIS, and MERIS sensors were used to evaluate and parameterize CDOM and DOC empirical algorithms using R_{rs} visible bands; specifically, the performance of two empirical algorithms, namely the D'Sa *et al.* [18] algorithm using the $R_{rs}(510)/R_{rs}(555)$ band ratio and the Maninno *et al.* [22] algorithm using the $R_{rs}(490)/R_{rs}(555)$ band ratios were used to derive $a_{CDOM}(412)$. Level 1A SeaWiFS LAC (local area coverage) data with spatial resolution of 1.1 km at nadir, and with daily temporal resolution were acquired from NASA Goddard Space Flight Center (<http://oceancolor.gsfc.nasa.gov/>). Level 1A data were processed up to Level 2 (L2) using the SeaWiFS Data Analysis System (SeaDAS) developed by NASA's Ocean Biology Processing Group (OBPG) version 6.0 and IDL 6.3 to derive R_{rs} bands at 490, 510 and 555 nm. As the field data set spanned the period corresponding to the operational period of three ocean color sensors, the empirical algorithms were evaluated for SeaWiFS as well as the MODIS/Aqua and MERIS/ENVISAT sensors. MODIS/Aqua Level 1A LAC (~1 km at nadir, daily temporal resolution) were obtained from the NASA's Ocean Color website and processed to Level 2 (L2) to retrieve R_{rs} bands at 488 nm and 555 nm using SeaDAS 6.0 software package. The atmospheric correction algorithm developed by Gordon and Wang [45] was used for SeaWiFS and MODIS to derive R_{rs} bands. Furthermore, R_{rs} bands using 1×1 and 3×3 pixel box size (1km/pixel at nadir) centered on the position of field measurements were chosen. Due to paucity of data points, a time window of ± 14 h between satellite match-ups and field sampling was set. R_{rs} bands extracted from a 5×5 pixel box for both SeaWiFS and MODIS were also examined, but this pixel box size was not used because of the spatial heterogeneity in coastal waters; therefore, a 3×3 pixel box was applied for extracting most data. In order to develop an empirical algorithm to retrieve CDOM and DOC with MERIS/ENVISAT (European Space Agency (ESA)), Level 1 reduced resolution (RR) data, with a spatial resolution of ~1.2 km and daily temporal resolution, were obtained from ESA (<http://merci-srv.eo.esa.int/merci/welcome.do>) and processed to Level 2 using SeaDAS 6.0 software package. R_{rs} bands at 510 nm and 560 nm were extracted from 1×1 and 3×3 pixel box size (1.2 km/pixel at nadir) with ± 14 h temporal window between satellite overpass and the time of field sampling for obtaining sufficient data points. Matchup comparisons between satellite derived estimates and *in situ* measurements of CDOM absorption and DOC concentrations were assessed using statistical criteria such as bias, root mean square error, scatter index and the coefficient of determination (Table 2).

Table 2. Equations used for calculating error statistics for evaluation of algorithms.

Statistical Estimator	Formula
Bias	$\frac{1}{N} \sum_{i=1}^N (y_i - x_i)$
Root mean square error	$\sqrt{\frac{1}{N} \sum_{i=1}^N (y_i - x_i)^2}$
Scatter-index	$\frac{1}{\bar{x}} \sqrt{\frac{1}{N} \sum_{i=1}^N [(y_i - \bar{y}) - (x_i - \bar{x})]^2}$

where y_i is satellite-derived values and x_i is field-measured values.

3. Results

3.1. CDOM, DOC and Salinity Relationships

In order to develop an empirical ocean color DOC algorithm using CDOM's optical signature as a proxy for DOC, the relationship between these two parameters was examined seasonally (*i.e.*, for summer and spring-winter periods) (Table 3). Based on the location of the field measurements, the MR discharge strongly influenced the relationships between DOC, CDOM and salinity during summer (August 2007, September 2007, August 2009), while spring-winter data (May 2007, February 2008) were significantly affected by the AR discharge. In summer, $a_{\text{CDOM}(412)}$, DOC concentration and salinity in surface waters ranged from 0.023 to 2.45 m^{-1} (S.D. = 0.66, geometric mean = 0.35, $n = 40$), 117 to 488 $\mu\text{mol}\cdot\text{C}\cdot\text{L}^{-1}$ ($214 \pm 95 \mu\text{mol}\cdot\text{C}\cdot\text{L}^{-1}$, $n = 40$), and 4.39 to 34.39 psu (mean = 24.67 ± 7.30 psu), respectively. During spring-winter study period, $a_{\text{CDOM}(412)}$ varied from 0.011 m^{-1} to 5.47 m^{-1} (S.D. = 1.38, geometric mean = 0.52; $n = 40$), the DOC concentration ranged from 56 to 739 $\mu\text{mol}\cdot\text{C}\cdot\text{L}^{-1}$ ($246 \pm 185 \mu\text{mol}\cdot\text{C}\cdot\text{L}^{-1}$; $n = 40$), and salinity exhibited a range from 0.43 to 35.9 psu (mean = 23.01 ± 12.21 psu, $n = 40$). Elevated values of DOC and CDOM observed in spring-winter period were likely due to out-welled CDOM-laden water from productive wetlands adjacent to the AR plume [46].

Table 3. Coefficients resulting from regression analysis between $a_{\text{CDOM}(412)}$, DOC, and salinity.

Parameter	Season	Slope (a)	Intercept (b)	R ²	N
DOC vs. $a_{\text{CDOM}(412)}$	Summer	137.22	124.20	0.90	39
DOC vs. $a_{\text{CDOM}(412)}$	Spring-winter	127.02	77.97	0.90	40
$a_{\text{CDOM}(412)}$ vs. salinity	Summer	-0.079	2.62	0.77	39
$a_{\text{CDOM}(412)}$ vs. salinity	Spring-winter	-0.076	2.78	0.86	40
DOC vs. salinity	Summer	-11.48	497.82	0.77	39
DOC vs. salinity	Spring-winter	-11.84	482.64	0.90	40

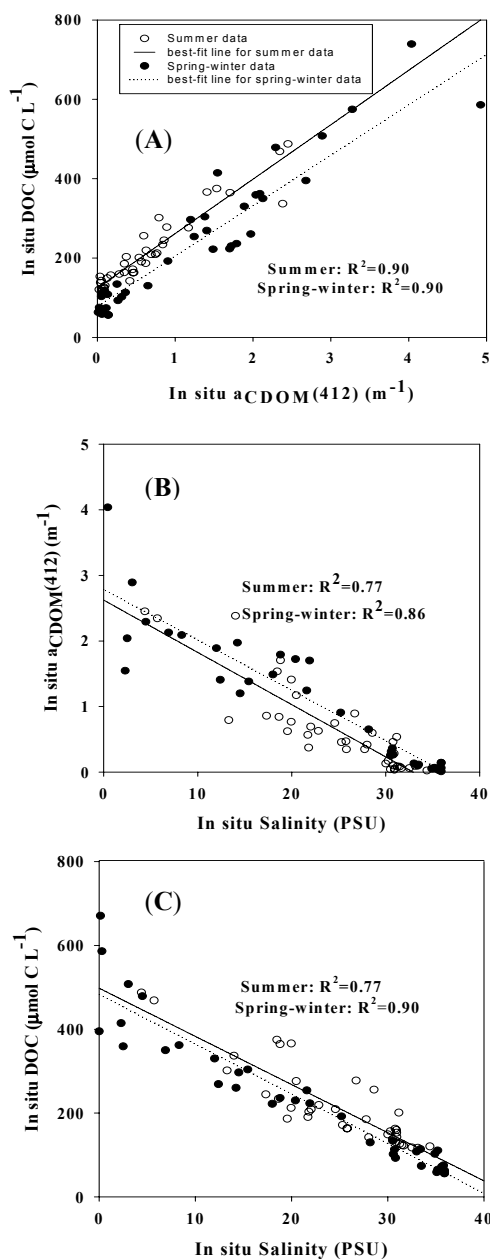
Linear equations were fitted to all variables ($y = a \times x + b$). In the DOC-CDOM relationship, $y = \text{DOC}$ and $x = a_{\text{CDOM}(412)}$; in the CDOM-salinity relationship, $y = a_{\text{CDOM}(412)}$ and $x = \text{salinity}$; in the DOC-salinity relationship, $y = \text{DOC}$ and $x = \text{salinity}$. All presented values are within interval Mean \pm 1 Stdev.

DOC concentrations were regressed against $a_{CDOM}(412)$ for spring-winter and summer periods to assess the seasonal relationship between DOC and CDOM. Results indicated strong conservative behavior between the two properties for both seasons (Equations (2) and (3); Figure 2(A), respectively). Regression analyses between $a_{CDOM}(412)$ and DOC concentration indicated high R^2 values (0.9) for both seasons with the intercept for the summer relationship (Equation (3)) being higher than that of spring-winter relationship (Equation (2)) (see Table 3).

$$DOC(\mu\text{mol C L}^{-1}) = 127.027 a_{CDOM}(412) + 77.97 \tag{2}$$

$$DOC(\mu\text{mol C L}^{-1}) = 137.22 a_{CDOM}(412) + 124.20 \tag{3}$$

Figure 2. Relationship between (A) *in situ* $a_{CDOM}(412)$ and *in situ* DOC in spring-winter and in summer; (B) *in situ* $a_{CDOM}(412)$ and *in situ* salinity in spring-winter and in summer; (C) *in situ* DOC and *in situ* salinity in spring-winter and in summer.



The high positive correlation between $a_{\text{CDOM}}(412)$ and DOC concentration suggests that these two properties behaved conservatively for the two time periods with mixing between the river and marine end members playing a critical role in the distribution of both CDOM and DOC. The seasonal relationships between $a_{\text{CDOM}}(412)$ and salinity (Table 3; Figure 2(B)) as well as between DOC concentration and salinity (Table 3; Figure 2(C)) exhibited strong linear inverse correlations for the summer and spring-winter periods. The inverse linear correlation between $a_{\text{CDOM}}(412)$ and salinity ($R^2 = 0.77$ in summer; $R^2 = 0.86$ in spring-winter) suggests strong river-derived or terrestrial sources; however, high CDOM and DOC concentrations due to riverine influences could be masking advective or autochthonous sources (e.g., *in situ* primary production) or removal processes (e.g., photooxidation, flocculation and sorption). These results indicate similar trends and consistency of a conservative behavior between CDOM and salinity in the northern Gulf of Mexico [40]. The seasonal variation in MR and AR discharges along with effects of mixing caused by energetic atmospheric events (*i.e.*, intrusion of cold fronts or storms) likely induces variability in CDOM optical properties and DOC concentration in the northern Gulf of Mexico [46–48] affecting biogeochemical cycles and the relationship between these two properties and salinity.

A strong negative correlation (Table 3; Figure 2(C)) exhibited between DOC and salinity indicates that terrestrial-derived DOC was conserved during the mixing of river and marine end member waters. The strong correlations between these three properties show the persistent influence of the MR and AR discharges on the CDOM distribution and geochemical cycle in the northern Gulf of Mexico (Coble, 2007). These results indicate that the first condition to derive DOC remotely and exclusively was met here (Figure 2). Table 4 represents the data used in the Figure 2. The data utilized to examine conservative behavior of DOC and CDOM were not used to evaluate and develop empirical algorithms in the following sections.

Table 4. Station locations, $a_{\text{CDOM}}(412)$, DOC, and salinity data used in Figure 2.

Date	Latitude	Longitude	CDOM	DOC	Salinity
Jul-2007	29.57	−92.04	1.536	375.00	18.47
	29.54	−92.08	1.409	365.83	19.97
	29.62	−91.99	0.792	301.50	13.30
	29.32	−89.94	1.172	276.17	20.49
Aug-2007	29.35	−89.91	0.894	277.42	26.72
	29.32	−89.94	0.597	255.75	28.57
Sep-2007	29.62	−91.99	2.450	487.50	4.39
	29.57	−92.04	2.345	468.58	5.71
	29.35	−89.91	1.706	364.33	18.81
Jun-2008	29.32	−89.94	2.381	336.67	14.02
	29.05	−90.02	0.692	208.83	22.03
	28.38	−89.47	0.083	123.42	31.48
	29.04	−89.49	0.624	186.58	19.56
	29.23	−89.88	0.470	163.00	25.77
	28.87	−90.48	0.173	156.42	30.27
	28.73	−91.00	0.348	185.08	27.76
	28.91	−90.02	0.537	201.00	31.16
	28.55	−89.47	0.051	142.75	30.95

Table 4. Cont.

Date	Latitude	Longitude	CDOM	DOC	Salinity
	28.91	−89.47	0.747	209.17	24.58
	29.18	−90.02	0.840	233.75	18.65
	28.72	−90.47	0.459	162.42	30.77
	28.71	−90.00	0.282	159.42	30.90
	28.55	−89.75	0.035	153.17	30.92
	28.91	−89.61	0.373	203.08	21.80
	29.05	−90.02	0.628	219.17	22.84
	28.55	−90.48	0.093	117.17	33.14
	28.53	−90.02	0.042	137.67	30.51
	28.72	−89.75	0.100	130.42	30.80
Sep-2009	28.93	−90.02	0.130	149.08	30.01
	28.38	−90.48	0.060	117.75	32.52
	28.72	−89.47	0.456	171.33	25.29
	29.05	−89.75	0.085	126.25	31.25
	28.98	−90.25	0.567	190.58	21.71
	28.73	−90.72	0.346	163.58	25.83
	28.38	−89.75	0.061	122.25	31.66
	28.91	−89.47	0.767	212.17	19.95
	29.18	−89.75	0.419	142.08	28.02
	29.04	−90.48	0.859	244.50	17.33
	28.53	−91.00	0.023	120.25	34.39

3.2. CDOM and DOC Empirical Algorithms: Validation and Development

3.2.1. Validation of Empirical Algorithms to Derive CDOM and DOC

The second condition for estimating DOC concentration using satellite ocean color sensors is to provide a robust relationship between R_{rs} band ratio and CDOM absorption coefficient to retrieve CDOM remotely. Then DOC concentration can be derived through this relationship and the CDOM-DOC relationship. The D'Sa *et al.* [18] SeaWiFS empirical algorithm developed using the relationship between *in situ* $a_{CDOM}(412)$ measurements and reflectance ratios during three field cruises in spring and fall of 2000 and March 2002 in the northern Gulf of Mexico was:

$$a_{CDOM}(412) = 0.227[(R_{rs}(510)/R_{rs}(555))]^{-2.022} \quad (4)$$

Equation (4) was applied to SeaWiFS data to obtain surface $a_{CDOM}(412)$ map for 6 February 2007 (Figure 3). The robustness of this algorithm was assessed by comparing satellite-estimated $a_{CDOM}(412)$ with *in situ* $a_{CDOM}(412)$ within ± 14 h of the satellite overpass. Match-up comparison illustrates a satisfactory trend and close agreement between satellite-derived and *in situ* $a_{CDOM}(412)$ for the study region (Figure 4(A)) with data being uniformly distributed along the one-to-one line. The algorithm was further quantified using bias function, root mean square error (RMSE), scatter-index (SI) and coefficient of determination (R^2) (Table 2). The statistical analysis revealed that the D'Sa *et al.* [18] algorithm performed well in the study area with relatively high R^2 (0.66), low RMSE (0.23), and low Bias (−0.045) (Table 5). The other empirical algorithm assessed was the algorithm which was

constructed by localizing the Mannino *et al.* (2008) [22] algorithm developed to retrieve $a_{CDOM}(412)$ from SeaWiFS in the US Middle Atlantic Bight. We localized the Mannino *et al.* [22] algorithm (hereafter, LM, which stands for the localized Mannino *et al.* (2008) algorithm) with regional data by constructing the relationship between satellite-derived R_{rs} band ratio (R_{rs490}/R_{rs555}) and *in situ* $a_{CDOM}(412)$ sampled in the northern Gulf of Mexico. The new relationship was applied to SeaWiFS imagery using SeaDAS 6.0 software to derive $a_{CDOM}(412)$. To validate the relationship, *in situ* $a_{CDOM}(412)$ values were compared with satellite-derived $a_{CDOM}(412)$ values within ± 14 h of the satellite overpass. This yielded $R^2 = 0.41$, RMSE = 0.4, and Bias = -0.21 (Table 5; Figure 4(B)). The *in situ* $a_{CDOM}(412)$ data used for matchup analysis were independent from the data utilized in the construction of the (R_{rs490}/R_{rs555})- $a_{CDOM}(412)$ relationship, and were similar to the data used in the D'Sa *et al.* [18] algorithm validation analysis. The matchup comparison results (Table 5; Figure 4(A,B)) indicate that the performance of an empirical algorithm utilizing $R_{rs}(490)/R_{rs}(555)$ for estimation of $a_{CDOM}(412)$ was less satisfactory than the D'Sa *et al.* [18] algorithm for the sample data used.

Figure 3. Surface colored dissolved organic matter (CDOM) absorption imagery ($a_{CDOM}(412)$) obtained using the D'Sa *et al.* [18] algorithm from SeaWiFS for 6 February 2007.

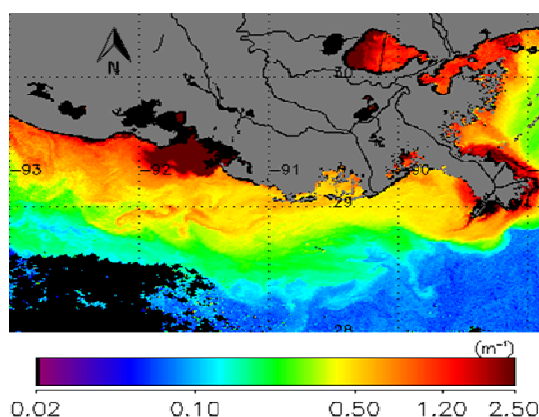


Figure 4. Scatter plots between *in situ* $a_{CDOM}(412)$ and SeaWiFS-derived $a_{CDOM}(412)$ obtained from (A) the D'Sa *et al.* [18]; and (B) LM algorithm. The 1-to-1 line is shown. Histogram of $a_{CDOM}(412)$ value estimated; (C) from D'Sa *et al.* [18] algorithm; (D) from LM algorithm.

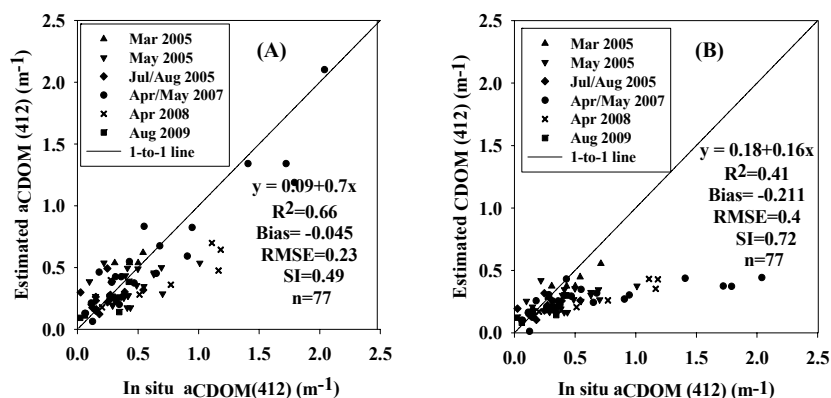


Figure 4. Cont.

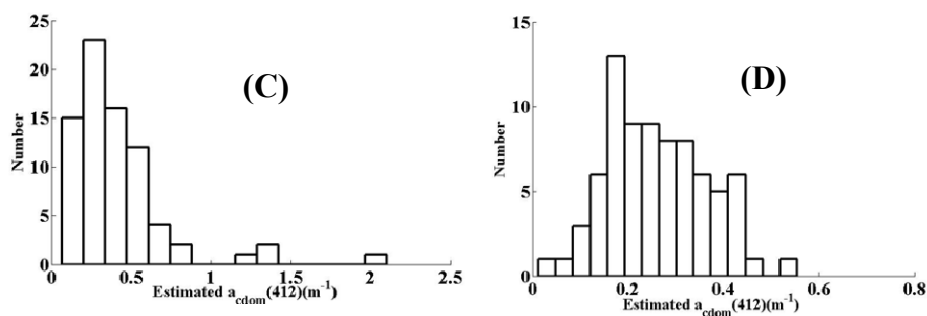


Table 5. Summary of error statistics derived from matchup comparisons between *in situ* and satellite-derived $a_{CDOM}(412)$ obtained from D’Sa *et al.* [18] and LM algorithms.

R _{rs} Band Ratio	R ²	RMSE	Bias	SI	Slope	Intercept	N *
R _{rs} 510/R _{rs} 555-D’Sa <i>et al.</i> (2006) algorithm	0.66	0.23	−0.045	0.49	0.70	0.09	77
R _{rs} 490/R _{rs} 555-LM algorithm	0.41	0.40	−0.211	0.72	0.16	0.18	77

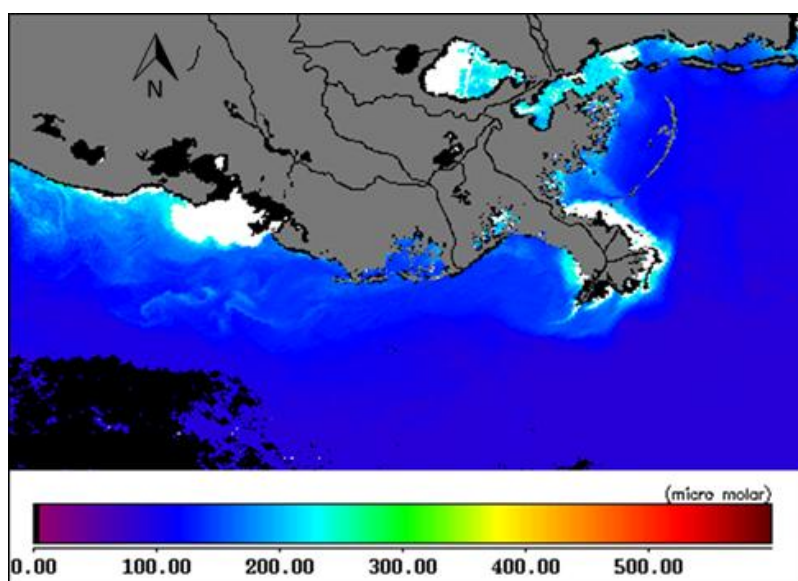
* N is the number of matchup observations.

Since the D’Sa *et al.* [18] SeaWiFS CDOM algorithm was found to be more robust for the estimation of $a_{CDOM}(412)$ in the northern Gulf of Mexico, this algorithm along with the CDOM-DOC relationship was used to derive DOC concentration remotely. The seasonal DOC algorithms were developed simply through the CDOM-DOC seasonal relationships (Equations (2) and (3)) and the D’Sa *et al.* [18] algorithm (Equation (4)). The DOC algorithms for the spring-winter and summer are:

$$DOC = 28.835 [R_{rs} (510)/(R_{rs} (555))]^{-2.022} + 77.97 \tag{5}$$

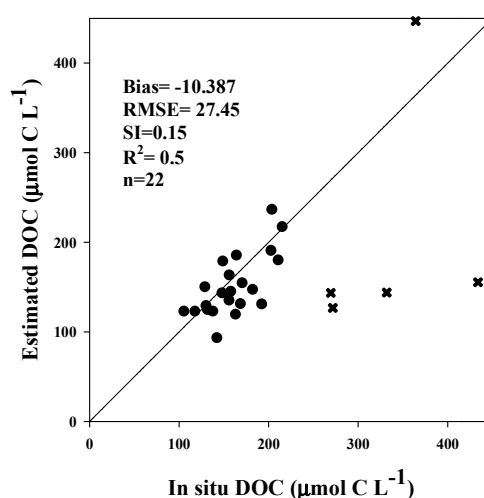
$$DOC = 31.148 [(R_{rs}(510)/(R_{rs} (555))]^{-2.022} + 124.20 \tag{6}$$

Figure 5. SeaWiFS-derived surface DOC concentration ($\mu\text{mol}\cdot\text{C}\cdot\text{L}^{-1}$) map for 6 February 2007. SeaWiFS-estimated DOC concentration higher than 250 μM which are outside the regression of the SeaWiFS-estimated DOC vs. field DOC masked in white color.



These algorithms were applied to SeaWiFS data to generate surface DOC concentration map (Figure 5). The performance of the newly developed DOC algorithm was examined just for the spring-winter period (Figure 6) due to the paucity of satellite-derived R_{rs} data in summer. The results of the statistical analysis indicate that retrieval of DOC concentration ($\mu\text{mol}\cdot\text{C}\cdot\text{L}^{-1}$) was reasonable (Bias = -10.38 , RMSE = 27.45 , SI = 0.15 , $R^2 = 0.5$, and $N = 22$). Surface DOC concentration obtained remotely using the DOC algorithm (Equation (5)) indicated a 7% percentage difference between SeaWiFS-estimated DOC and field DOC for spring-winter period. However, algorithm performance was found to degrade at elevated DOC concentrations ($>250 \mu\text{mol}\cdot\text{C}\cdot\text{L}^{-1}$) and in shallower nearshore and river plume waters.

Figure 6. Match-up comparison between the SeaWiFS-derived DOC and *in situ* DOC for the spring-winter period. The diagonal line is the 1:1 line. Cross symbols (\times) show the outliers data.



3.2.2. CDOM and DOC Empirical Algorithms for MODIS and MERIS Sensors

R_{rs} values at visible bands were derived from MODIS and MERIS to use as inputs to the empirical algorithms for CDOM and DOC. The R_{rs} band ratios used were $R_{rs}(488)/R_{rs}(555)$ for MODIS-Aqua and $R_{rs}(510)/R_{rs}(560)$ for MERIS-Envisat with wavebands chosen similar to the D'Sa *et al.* [18] and Mannino *et al.* [22]. The band ratio algorithms were regressed against coincident *in situ* $a_{CDOM}(412)$ measured within ± 14 time difference for MODIS and MERIS overpasses. Non-linear three-parameter exponential decay curves ($R^2 = 0.68$ for MODIS, $R^2 = 0.67$ for MERIS) (Figures 7(A) and 8(A)) exhibited higher correlation than the log-transformed R_{rs} band ratios plotted against log-transformed values of *in situ* $a_{CDOM}(412)$ ($R^2 = 0.66$ for MODIS, $R^2 = 0.5$ for MERIS) (Figures 7(B) and 8(B)). CDOM absorption coefficient can thus be retrieved using the R_{rs} band ratios:

$$a_{CDOM}(412) = \ln[(R_{rs} \text{ ratio} - A)/B]/(-C) \quad (7)$$

Table 6 presents R_{rs} ratio and coefficient values (A , B , and C) for MODIS and MERIS. The regional CDOM empirical algorithms were applied to MODIS and MERIS data (Figure 9(A,B)) to obtain surface CDOM absorption maps. The black regions in the CDOM images could be due to failure of the atmospheric correction algorithm in coastal and turbid waters. In addition, the regions along the coast

and estuaries exhibit high CDOM/DOC concentrations, where the MODIS/MERIS algorithms fail to estimate CDOM/DOC most likely due to interference by sediments and chlorophyll. These CDOM empirical relationships were evaluated using *in situ* $a_{CDOM}(412)$ data which were independent from the data utilized for algorithm development (Figure 9(C,D)). The validation matchup comparison between *in situ* and satellite-derived $a_{CDOM}(412)$ illustrates estimation of $a_{CDOM}(412)$ with Bias = 0.093, RMSE = 0.176, and $R^2 = 0.4$ for MODIS, and Bias = 0.089, RMSE = 0.3, $R^2 = 0.42$ for MERIS (Table 7). We excluded outliers to improve the evaluation analyses (Figure 9(C,D)) (see Discussion). The DOC retrieval algorithms for both MODIS and MERIS were constructed by combining the $a_{CDOM}(412)$ - R_{rs} relationship (Equation (7)) with seasonal $a_{CDOM}(412)$ -DOC relationships (Equations (2) and (3)). The resulting seasonal DOC- R_{rs} relationships for the spring-winter and the summer seasons, respectively, are:

$$DOC = 127.027 \ln [(R_{rs} \text{ ratio} - A)/B]/(-C) + 77 \tag{8}$$

$$DOC = 137.22 \ln[(R_{rs} \text{ ratio} - A)/B]/(-C) + 124.20 \tag{9}$$

Figure 7. MODIS-derived R_{rs} band ratio (488 nm and 555 nm) plotted against *in situ* surface CDOM absorption at 412 nm (A) exponential decay model and (B) logarithmic model.

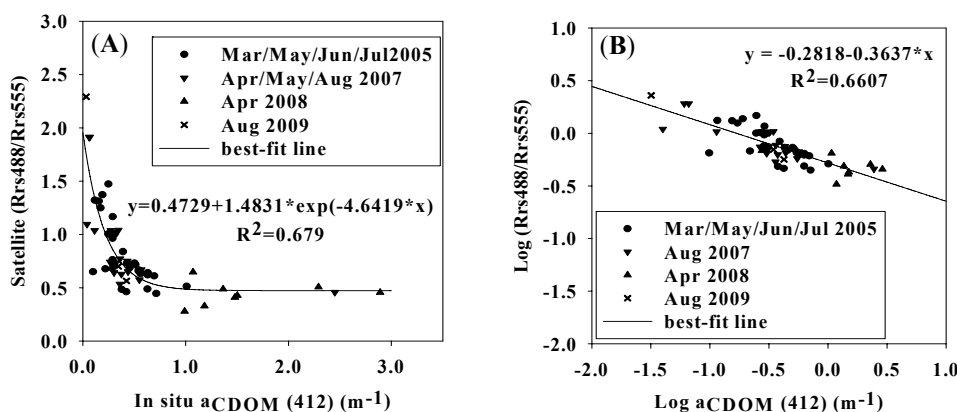


Figure 8. MERIS-derived R_{rs} band ratio (510 nm and 560 nm) plotted against *in situ* surface CDOM absorption at 412 nm (A) exponential decay model and (B) logarithmic model.

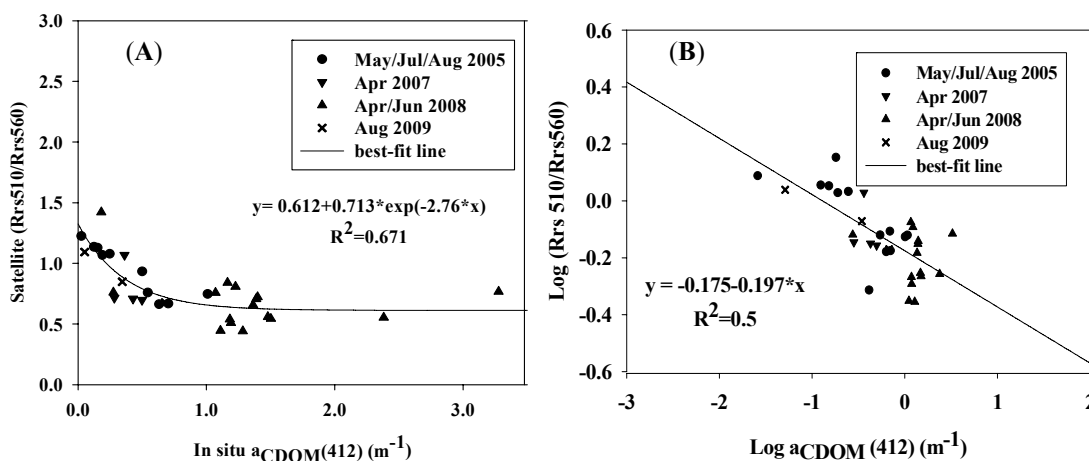


Figure 9. CDOM absorption map ($a_{CDOM}(412)$) for 6 February 2007 using (A) the MODIS algorithm; (B) the MERIS algorithm; scatter plots between; (C) MODIS-derived $a_{CDOM}(412)$ and *in situ* surface $a_{CDOM}(412)$; and (D) MERIS-derived $a_{CDOM}(412)$ and *in situ* surface $a_{CDOM}(412)$. CDOM values higher than 1.5 m^{-1} estimated by MODIS and MERIS which are outside the regression of the MODIS/MERIS-estimated CDOM vs. field CDOM masked in white color. Black regions in the coastal and turbid waters in the CDOM images are likely due to atmospheric correction failure. Cross symbols (*) on the plots show outlier data.

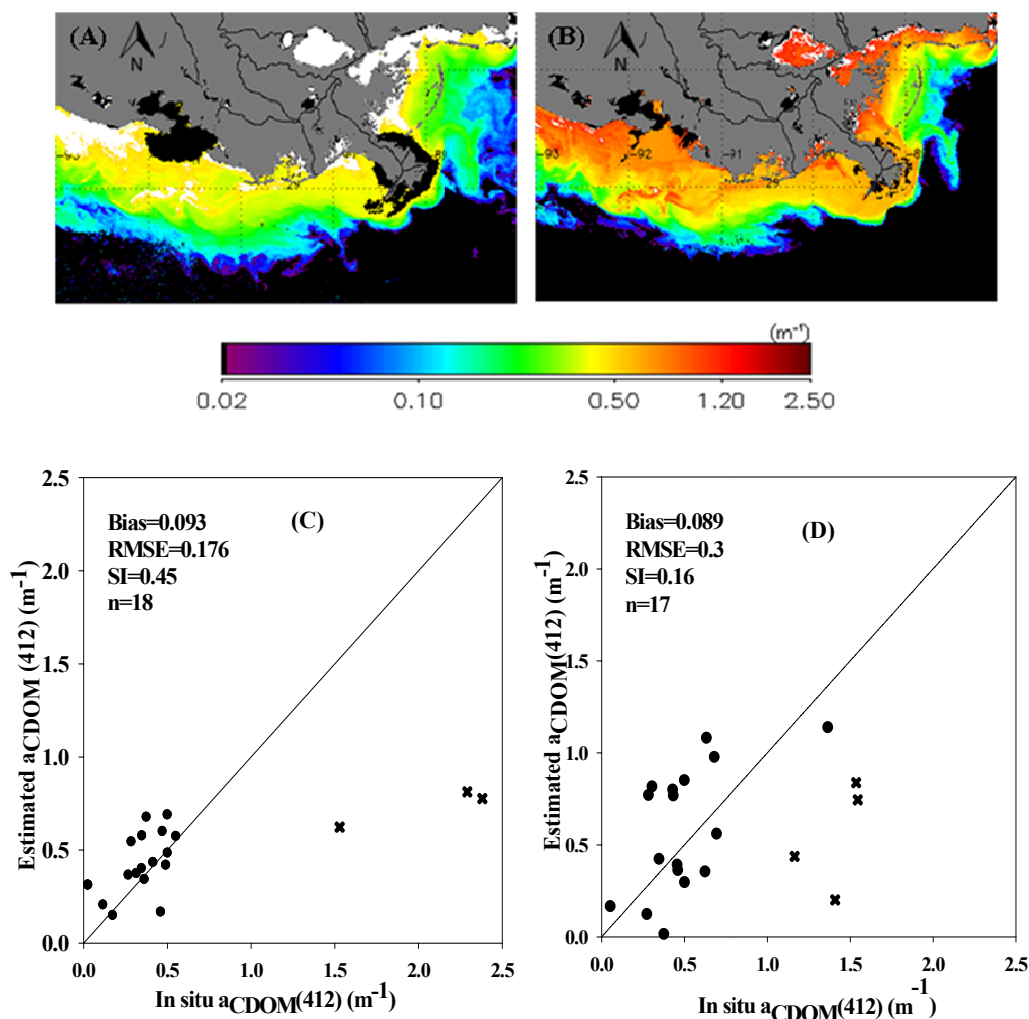


Table 6. Summary of fitted coefficients for the regional MODIS and MERIS empirical algorithm illustrated in Figures 7 and 8 for CDOM and DOC retrievals. Presented coefficients are fitted into the seasonal DOC algorithm.

Product	Satellite	Fitting Curve	R _{rs} Band Ratio	A	B	C	R ²
$a_{CDOM}(412)$	MODIS	3 parameter exponential decay	488/555	0.472	1.48	4.64	0.67
$a_{CDOM}(412)$	MERIS	3 parameter exponential decay	510/560	0.612	0.713	2.76	0.67

Table 7. Summary of error statistics obtained from validation matchup comparisons for $a_{\text{CDOM}}(412)$ and DOC derived from MODIS and MERIS for the summer and spring-winter seasons.

Products	Bias	RMSE	SI	R^2	Slope	Intercept	N
$a_{\text{CDOM}}(412)$ _MODIS	0.093	0.176	0.45	0.40	0.55	0.24	18
$a_{\text{CDOM}}(412)$ _MERIS	0.089	0.300	0.16	0.40	0.70	0.23	17
DOC_MODIS_summer	2.420	26.69	0.15	0.52	0.61	66.18	25
DOC_MERIS_summer	5.300	30.02	0.17	0.58	0.39	109.15	19
DOC_MODIS_spring-winter	-13.67	32.29	0.22	0.40	0.43	56.96	25
DOC_MERIS_spring-winter	-3.500	44.22	0.21	0.72	0.99	-2.39	7

The R_{rs} band ratios and coefficients for both MODIS and MERIS are presented in Table 6. Surface DOC concentration maps were obtained by applying the newly developed DOC algorithms to MODIS and MERIS data (Figure 10(A,B)). To test the performance of the DOC algorithms for each sensor, the *in situ* DOC concentrations ($\mu\text{mol}\cdot\text{C}\cdot\text{L}^{-1}$) were compared with MODIS and MERIS-derived DOC ($\mu\text{mol}\cdot\text{C}\cdot\text{L}^{-1}$) (Figure 11(A–D)). The matchup comparisons showed estimation of DOC with Bias = -13.67, RMSE = 32.29, SI = 0.22, $R^2 = 0.4$, and N = 25 for MODIS, and Bias = -3.5, RMSE = 44.22, SI = 0.21, $R^2 = 0.72$, and N = 7 for MERIS during the spring-winter period (Table 7). The statistical parameters obtained from validation of DOC for MODIS (Bias = 2.42, RMSE = 26.59, SI = 0.15, $R^2 = 0.52$, and N = 25) and for MERIS (Bias = 5.3, RMSE = 30.02, SI = 0.17, $R^2 = 0.58$, and N = 19) during the summer period are shown in Table 7. The statistical analysis verifies acceptable performance of the DOC algorithm for MERIS in the northern Gulf of Mexico in both the summer and spring-winter periods.

The empirical algorithm for CDOM is: $a_{\text{CDOM}}(412) = \ln[(R_{rs} \text{ ratio} - A)/B]/(-C)$, and the equations for seasonal DOC are: DOC = 127.027 $\ln[(R_{rs} \text{ ratio} - A)/B]/(-C) + 77$ for the spring-winter season, DOC = 137.22 $\ln[(R_{rs} \text{ ratio} - A)/B]/(-C) + 124.20$ for summer. The coefficients are presented in Table 6.

Figure 10. (A) MODIS-derived surface DOC ($\mu\text{mol}\cdot\text{C}\cdot\text{L}^{-1}$) concentration for 6 February 2007; (B) MERIS-derived surface DOC ($\mu\text{mol}\cdot\text{C}\cdot\text{L}^{-1}$) for the same date. MODIS/MERIS estimated DOC concentrations higher than 250 μM which are outside the regression of the MODIS/MERIS-estimated DOC vs. field DOC masked in white color.

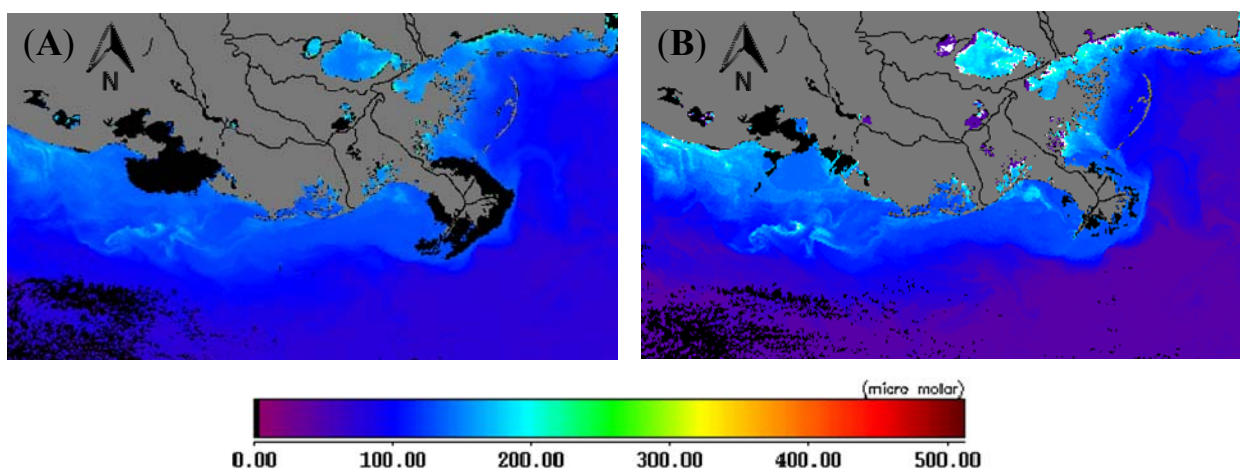
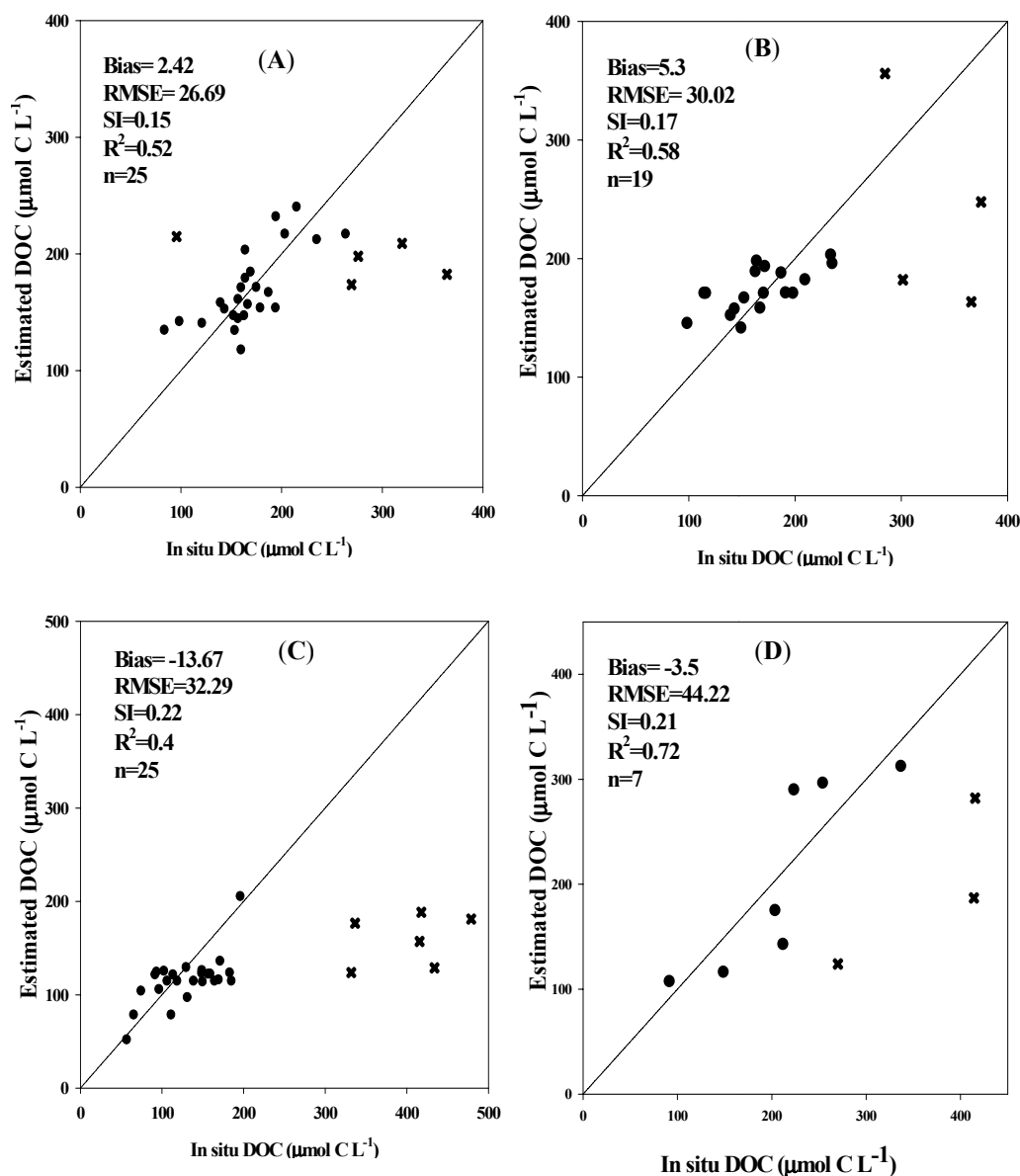


Figure 11. Scatter plots of satellite-derived *versus in situ* DOC ($\mu\text{mol}\cdot\text{C}\cdot\text{L}^{-1}$) for (A) MODIS in summer; (B) MERIS in summer; (C) MODIS in the spring-winter season; (D) MERIS in the spring-winter season. Cross symbols (\times) show the outlier data.



4. Discussion

4.1. CDOM, Salinity and DOC Relationship

The conservative behavior of CDOM and DOC were examined through the correlations between DOC, CDOM, and salinity. Seasonal variability in CDOM and DOC concentration is highly dependent on the MR and AR discharges [18,46,49]. Naik *et al.* [49] reported that on the Atchafalaya shelf, CDOM dominates the total light absorption when Atchafalaya River flow is high, while non-algal particles (NAP) play a more important role contributing to total light absorption during low-flow conditions. Chen and Gardner [46] observed high concentrations of CDOM and DOC during high-flow conditions in the Mississippi and Atchafalaya River plume regions, as well as their seasonal variability linked to water's residence time and plant growth cycles in the watershed. We observed that *in situ*

DOC concentration in the lower Atchafalaya River was ~35% on average higher than DOC concentration in the lower MR during the spring-winter period and is similar (~20%–30%) to the results reported by Wang *et al.* [50] for April 2001. The elevated DOC and CDOM in the lower Atchafalaya River plume is likely due to the interaction of the Atchafalaya River with the adjacent productive and extensive salt marshes, wetlands and bayous, while in comparison such interactions are less for the Mississippi River [37,46]. The strong inverse linear correlation between $a_{\text{CDOM}}(412)$ and salinity observed in summer ($R^2 = 0.77$), and in the spring-winter period ($R^2 = 0.86$) suggests that terrestrial allochthonous CDOM behaved conservatively in the study area. Sampling in low salinity, high CDOM waters during summer likely masked the effects of light-induced photobleaching. The strong correlation between CDOM absorption coefficient at 412 nm and DOC concentration shows that the distribution of DOC was also highly influenced by physical mixing between two-end members, indicating conservative behavior of DOC. However, the relationship during summer suggests loss of CDOM in comparison to DOC.

4.2. CDOM and DOC Retrieval Algorithms

In assessing the performance of two empirical CDOM algorithms for SeaWiFS, it was found that the percentage differences between SeaWiFS-estimated CDOM and field CDOM associated with the D'Sa *et al.* [18] and the LM algorithm for CDOM retrieval were 10% and 61%, respectively. Poor performance of the LM algorithm could be due to an interference from chlorophyll-a and particulate organic carbon (POC) in the $R_{rs}(490)/R_{rs}(555)$ ratio. In comparison, the R_{rs} band ratio ($R_{rs}(510)/R_{rs}(555)$) proposed by D'Sa *et al.* [18] is less affected by chlorophyll-a and POC [51–53] exhibiting high accuracy in CDOM retrievals for summer, while spring-winter was not evaluated due to lack of data. These results also suggest that the DOC algorithm based on D'Sa *et al.* [18] R_{rs} band ratio performs well in the northern Gulf of Mexico.

The matchup comparison between *in situ* $a_{\text{CDOM}}(412)$ and MODIS-derived CDOM showed an overestimation of CDOM by MODIS (24%, the percentage difference between satellite estimated CDOM and field CDOM) which could be due to interference by chlorophyll-a on the $R_{rs}(488)/R_{rs}(555)$ band ratio used for $a_{\text{CDOM}}(412)$ retrieval. However, other factors such as the time difference between satellite overpass and field measurement, pixel box size, and errors and uncertainties associated with satellite-derived R_{rs} used to develop the empirical algorithm can accentuate these discrepancies. Since CDOM concentration is highly variable spatially and temporally in our study area, appropriate available time difference (less than 5 h) and pixel box size (1×1) could improve these disparities.

The empirical algorithm developed for MODIS failed for $a_{\text{CDOM}}(412)$ values larger than $1.5 \text{ (m}^{-1}\text{)}$ in CDOM-rich coastal and estuarine waters. Strong underestimation of MODIS-derived CDOM values (for values larger than 1.5 m^{-1}) in coastal waters could be related to the sediment resuspension and errors associated with atmospheric correction algorithms in turbid waters [54]. In addition, Osburn *et al.* [55] hypothesized that intermolecular charge transfer may be disrupted in CDOM-rich sources that are exposed to increasing salinities. Furthermore, it is more likely that the selected pixel box size and time difference, which were limited by cloud coverage, sun glint, and lack of swath, exacerbated the inaccuracy of CDOM retrieval. Table 8 presents the stations' information along with

selected pixel box size and time difference for some stations mainly located at the mouth of Barataria and Vermilion Bays that were excluded as outliers for the validation analysis.

Table 8. Summary of outlier stations excluded from CDOM matchup comparison for MODIS.

Station#	1	2	3	4	5
Date	20080209	20080602	20080209	20070913	20080602
Latitude	29.573	29.352	29.539	29.350	29.316
Longitude	-92.043	-89.913	-92.080	-89.910	-89.942
<i>In situ</i> $a_{\text{CDOM}}(412)$	2.292	2.660	1.529	1.706	2.381
MODIS-derived $a_{\text{CDOM}}(412)$	0.812	0.869	0.623	0.425	0.777
Pixel box size	3 × 3	3 × 3	1 × 1	3 × 3	3 × 3
Time difference (h)	+10	-5	+7	-4	-12

As illustrated in Figure 11(A), the algorithm proposed for DOC retrieval with MODIS performs relatively well for summer, while MODIS-estimated DOC concentration was underestimated (11%, the percentage difference between MODIS-estimated DOC and field DOC) during the spring-winter period. Considering the locations of stations during the spring-winter period which were mainly in shallow waters, this underestimation could be attributed to the sediment resuspension associated with cold front passage during spring-winter season [56]. The sediment resuspension process, and the desorption of organic matter from resuspended particles and pore waters [57] contaminate remote sensing reflectance and affects light availability leading to the underestimation of DOC concentration. Since the spring-winter field data were sampled mostly from shallow areas, the effects of sediment resuspension could have been enhanced. Also, the optically inactive fraction of DOC that cannot be measured by satellite could have contributed to the elevated DOC concentration leading to further underestimation of DOC by MODIS.

The influence of cold fronts on DOC concentration has been examined by comparing the occurrences of cold fronts and the time of DOC measurements. It appears that cold front passage increases DOC concentration resulting in less agreement between measured and satellite-derived DOC estimates, while the DOC field measurement corresponding to the time when no cold front occurred exhibited higher agreement. For example on 18 April 2008, for the station located at Tiger Shoal off the Atchafalaya Bay, the *in situ* DOC sampling coincided with the passage of a cold front. The measured DOC concentration was $218.50 \mu\text{mol}\cdot\text{C}\cdot\text{L}^{-1}$, while MODIS-derived DOC concentration was $125.84 \mu\text{mol}\cdot\text{C}\cdot\text{L}^{-1}$ (53% underestimation). In contrast, on 16 April 2008 with no cold front, *in situ* DOC concentration at a station close to the former station was $170.9 \mu\text{mol}\cdot\text{C}\cdot\text{L}^{-1}$, while MODIS-derived DOC concentration was $136.55 \mu\text{mol}\cdot\text{C}\cdot\text{L}^{-1}$ (17% underestimation). This increase in DOC concentration during cold fronts is likely due to resuspension of sediments [58] and the associated high DOC [59] pore waters in northern Gulf of Mexico shelf sediments.

The better retrieval of $a_{\text{CDOM}}(412)$ using $R_{\text{rs}}(510)/R_{\text{rs}}(560)$ for MERIS than for MODIS (the percentage differences of 16% for MERIS and of 24% for MODIS) could be attributed to the use of the 510 nm band in constructing the CDOM algorithm which is less affected by chlorophyll-a than the 488 nm band used in the MODIS CDOM algorithm. However, the MERIS algorithm overestimated CDOM values by the percentage difference of 16%. This overestimation could be attributed to some factors including sediment resuspension over the shallow area, presence of chlorophyll-a, time gap,

and pixel box size for CDOM retrievals. The location of stations excluded from the MERIS CDOM algorithm evaluation and considered as outliers (Figure 12) are detailed for five selected stations (Table 9). Stations located at Louisiana Bight are highly affected by MR sediment plume as a result of westward coastal current and clockwise gyre generally present in the region [60,61], whereas stations located in the Atchafalaya-Vermilion Bay region are influenced by AR sediment plume. Optical interference of suspended sediments and other photoreactive constituents in surface waters can interfere with the CDOM signal received by the sensor, and could lead to significant errors in CDOM estimates by MERIS sensor. Also, large time gaps between satellite overpasses and *in situ* sampling, and pixel box size used in CDOM retrievals could likely further deteriorate the performance of the CDOM algorithm in these dynamic coastal waters (Table 9).

Figure 12. (●) indicates location of outliers excluded from CDOM matchup comparison for MERIS, and (◆) denotes location of stations used for evaluation of MERIS DOC algorithm.

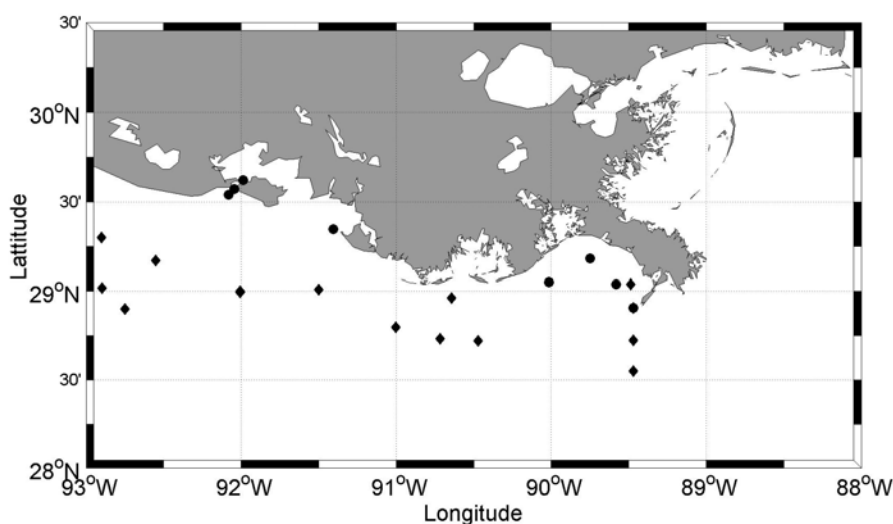


Table 9. Summary of outlier stations excluded from CDOM matchup comparison for MERIS.

Station#	1	2	3	4	5
Date	20090819	20080406	20080407	20070717	20050523
Latitude	28.90	29.573	29.05	29.57	29.03
Longitude	-89.47	-92.04	-90.01	-92.04	89.58
<i>In situ</i> $a_{CDOM}(412)$	0.74	3.27	1.22	1.53	0.09
MERIS-derived $a_{CDOM}(412)$	0.31	0.59	0.50	0.83	0.43
Pixel box size	3 × 3	3 × 3	1 × 1	3 × 3	1 × 1
Time difference (h)	10	24	6	14	8

MERIS estimates of DOC shows the percentage differences of 3% and 1.7% for summer and spring-winter respectively, and compared to the error associated with MODIS, the MERIS estimation shows greater accuracy. This could be due to the geographical location of stations used for MERIS DOC algorithm evaluation. While the stations used for evaluation of the DOC algorithm for MODIS were mostly located in shallow water, the stations used for testing the DOC algorithm for MERIS were located mostly in deeper water (Figure 12, for summer time). The stations' location in deep water suggests that satellite derived band ratios were less affected by coastal water turbidity. Similar to

MODIS, outlier points located in estuarine and coastal areas were excluded from DOC algorithm evaluation analysis. The DOC algorithm failed at these stations due to the effect of the same factors that caused MODIS DOC algorithm failure.

5. Summary and Conclusion

The relationship between CDOM and DOC, as well as an assessment of CDOM and DOC retrieval algorithms using SeaWiFS, MODIS, and MERIS were addressed in this study. Field measured CDOM and DOC obtained from different research cruises covering areas over the Louisiana shelf in 2005 and from 2007 to 2009 were employed to evaluate and develop CDOM and DOC retrieval algorithms. Conservative DOC and CDOM behavior for both summer and spring-winter periods were observed in the study area. These conservative relationships were used to develop empirical algorithms to derive DOC concentration from satellite ocean color sensors.

In comparing the D'Sa *et al.* [18] algorithm with the LM algorithm for CDOM estimation and further for DOC estimation, the D'Sa *et al.* [18] SeaWiFS algorithm performed relatively well. Similar processes were followed to develop a DOC algorithm for MODIS and MERIS sensors. For MODIS, $R_{rs}(488)/R_{rs}(555)$ values were obtained from satellite data and correlated with $a_{CDOM}(412)$, while for MERIS, $R_{rs}(510)/R_{rs}(560)$ values were used to construct a band ratio empirical algorithm. A comparison of satellite-derived with *in situ* $a_{CDOM}(412)$ revealed that both MODIS and MERIS tend to overestimate CDOM values $< 1.5 \text{ m}^{-1}$, and both algorithms failed for CDOM values $> 1.5 \text{ m}^{-1}$. Several factors may contribute to these discrepancies such as optical interference of chlorophyll-a, time difference between satellite overpass and field measurements, and the selected pixel box size. In addition, the seasonal relationship between $a_{CDOM}(412)$ and DOC was combined with the $a_{CDOM}(412)$ - R_{rs} ratio to construct DOC seasonal empirical algorithms. Then satellite-derived DOC values were correlated against *in situ* DOC values to test their performance. In summer, both sensors performed reasonably well, while in the spring-winter period there was a tendency for underestimation of DOC particularly for MODIS, likely due to sediment resuspension by cold front intrusions or time difference between *in situ* and satellite passes.

The approach followed in this study was based on available field and satellite data. As mentioned in the discussion section, some spatial and temporal limitations associated with available data introduced significant errors and uncertainties. In order to develop more robust empirical algorithms to estimate DOC concentration and gain insight about DOC dynamics, future measurements of physical and optical properties should be obtained at high temporal and spatial resolution and coincident with satellite overpasses. Since SeaWiFS and MERIS are no longer operational, and MODIS is exceeding its nominal six-year design lifetime, developing new algorithms for new sensors and their validation against the *in situ* data is required.

Acknowledgements

The authors acknowledge support provided by a NASA grant NNX09AR7OG. E. D'Sa acknowledges partial support from the Bureau of Ocean Energy Management Cooperative Agreement (1435-0104CA32806) and a NASA grant (NNA07CN12A).

References

1. Hansell, D.A.; Carlson, C.A. Biogeochemistry of total organic carbon and nitrogen in the Sargasso Sea: Control by convective overturn. *Deep-Sea Res.* **2001**, *48*, 1649–1667.
2. Jiao, N.; Herndl, G.J.; Hansell, D.A.; Benner, R.; Kattner, G.; Wilhelm, S.W.; Kirchman, D.L.; Weinbauer, M.G.; Luo, T.; Chen, F.; *et al.* Microbial production of recalcitrant dissolved organic matter: Long-term carbon storage in the global ocean. *Nat. Rev. Microbiol.* **2010**, *8*, 593–599.
3. Ogawa, H.; Tanoue, E. Dissolved organic matter in oceanic waters. *J. Oceanogr.* **2003**, *59*, 129–147.
4. Gandhi, H.; Wiegner, T.N.; Ostrom, P.H.; Kaplan, L.A.; Ostrom, N.E. Isotopic (^{13}C) analysis of dissolved organic carbon in stream water using an elemental analyzer coupled to a stable isotope mass spectrometer. *Rapid Commun. Mass Spectrom.* **2004**, *18*, 903–906.
5. Fichot, C.G.; Benner, R. A novel method to estimate DOC concentrations from CDOM absorption coefficients in coastal waters. *Geophys. Res. Lett.* **2011**, doi: 10.1029/2010GL046152.
6. Coble, P.G. Marine optical biogeochemistry: The chemistry of ocean color. *Chem. Rev.* **2007**, *107*, 402–418.
7. Del Castillo, C.E.; Miller, R.L. On the use of ocean color remote sensing to measure the transport of dissolved organic carbon by the Mississippi River Plume. *Remote Sens. Environ.* **2008**, *112*, 836–844.
8. Griffin, C.G.; Frey, K.E.; Rogan, J.; Holmes, R.M. Spatial and interannual variability of dissolved organic matter in the Kolyma River, East Siberia, observed using satellite imagery. *J. Geophys. Res.* **2011**, doi:10.1029/2010JG001634.
9. Coble, P.G.; Hu, C.; Gould, R.W., Jr.; Chang, G.; Wood, A.M. Colored dissolved organic matter in the coastal ocean. *Oceanography* **2004**, *17*, 50–59.
10. D'Sa, E.J.; Miller, R.L.; Mckee, B.A. Suspended particulate matter dynamics in coastal waters from ocean color: Application to the northern Gulf of Mexico. *Geophys. Res. Lett.* **2007**, doi: 10.1029/2007GL031192, .
11. Carder, K.L.; Chen, F.R.; Lee, Z.P.; Hawes, S.K.; Kamykowski, D. Semianalytic Moderate-Resolution Imaging Spectrometer algorithms for chlorophyll-a and absorption with bio-optical domains based on nitrate-depletion temperatures. *J. Geophys. Res.* **1999**, *104*, 5403–5421.
12. Hoge, F.E.; Wright, C.W.; Lyon, P.E.; Swift, R.N.; Yungel, J.K. Inherent optical properties imagery of the western North Atlantic Ocean: Horizontal spatial variability of the upper mixed layer. *J. Geophys. Res.* **2001**, *106*, 129–140.
13. Maritorena, S.; Siegel, D.A.; Peterson, A. Optimization of a semi-analytical ocean color model for global scale applications. *Appl. Opt.* **2002**, *41*, 2705–2714.
14. Siegel, D.A.; Maritorena, S.; Nelson, N.B.; Hansell, D.A.; Lorenzi-Kayser, M. Global distribution and dynamics of colored dissolved and detrital organic materials. *J. Geophys. Res.* **2002**, doi: 10.1029/2001JC000965.
15. Bricaud, A.; Morel, A.; Prieur, L. Absorption by dissolved organic matter in the sea (yellow substance) in the UV and visible domains. *Limnol. Oceanogr.* **1981**, *26*, 43–53.
16. Morel, A.; Prieur, L. Analysis of variations in ocean color. *Limnol. Oceanogr.* **1977**, *22*, 709–722.

17. IOCCG. *Status and Plans for Satellite Ocean Color Missions: Considerations for Complementary Missions*; Report Number 2; IOCCG: Dartmouth, NS, Canada, 1999; p. 5.
18. D'Sa, E.J.; Miller, R.L.; Del Castillo, C. Bio-optical properties and ocean color algorithms for coastal waters influenced by the Mississippi River during a cold front. *Appl. Opt.* **2006**, *45*, 7410–7428.
19. Kahru, M.; Mitchell, B.G. Seasonal and nonseasonal variability of satellite-derived chlorophyll and colored dissolved organic matter concentration in the California Current. *J. Geophys. Res.* **2001**, *106*, 2517–2529.
20. D'Sa, E.J.; Miller, R.L. Bio-optical properties in waters influenced by the Mississippi River during low flow conditions. *Remote Sens. Environ.* **2003**, *84*, 538–549.
21. Johannessen, S.C.; Miller, W.L.; Cullen, J.J. Calculation of UV attenuation and colored dissolved organic matter absorption spectra from measurements of ocean color. *J. Geophys. Res.* **2003**, doi: 10.1029/2000JC000514.
22. Mannino, A.; Russ, M.E.; Hooker, S.B. Algorithm development and validation for satellite-derived distributions of DOC and CDOM in the US Middle Atlantic Bight. *J. Geophys. Res.* **2008**, *113*, 1–19.
23. Twardowski, M.S.; Lewis, M.; Barnard, A.; Zaneveld, J.R.V. In-Water Instrumentation and Platforms for Ocean Color Remote Sensing Applications. In *Remote Sensing of Coastal Aquatic Environments*; Miller, R., Del Castillo, C., McKee, B., Eds.; Springer: Dordrecht, The Netherlands, 2005; pp. 69–100.
24. Zhu, W.; Yu, Q.; Tian, Y.Q.; Chen, R.F.; Gardner, G.B. Estimation of chromophoric dissolved organic matter in the Mississippi and Atchafalaya river plume regions using above-surface hyperspectral remote sensing. *J. Geophys. Res.* **2011**, doi: 10.1029/2010JC006523.
25. Vodacek, A.; Hoge, F.E.; Swift, R.N.; Yungel, J.K.; Peltzer, E.T.; Blough, N.V. The use of *in situ* and airborne fluorescence measurements to determine UV absorption coefficients and DOC concentrations in surface waters. *Limnol. Oceanogr.* **1995**, *40*, 411–415.
26. Ferrari, G.M. The relationship between chromophoric dissolved organic matter and dissolved organic carbon in the European Atlantic coastal area and in the West Mediterranean Sea (Gulf of Lions). *Mar. Chem.* **2000**, *70*, 339–357.
27. Rochelle-Newall, E.J.; Fisher, T.R. Production of chromophoric dissolved organic matter fluorescence in marine and estuarine environments: An investigation into the role of phytoplankton. *Mar. Chem.* **2002**, *77*, 7–21.
28. Del Vecchio, R.; Blough, N.V. Spatial and seasonal distribution of chromophoric dissolved organic matter and dissolved organic carbon in the Middle Atlantic Bight. *Mar. Chem.* **2004**, *89*, 169–187.
29. Kowalczyk, P.; Zablocka, M.; Sagan, S.; Kulinski, K. Fluorescence measured *in situ* as a proxy of CDOM absorption and DOC concentration in the Baltic Sea. *Oceanologia* **2010**, *52*, 431–471.
30. Bianchi, T.S.; Allison, M.A. Large-river delta-front estuaries as natural “recorders” of global environmental change. *Proc. Nat. Acad. Sci. USA* **2009**, *106*, 8085–8092.
31. Van Der Leeden, F.; Troise, F.L.; Todd, D.K. *The Water Encyclopedia*, 2nd ed.; Lewia: Chelsea, MI, USA, 1990.
32. Milliman, J.D. Flux and Fate of Fluvial Sediment and Water in Coastal Seas. In *Ocean Margin Processes in Global Change*; Mantoura, R.F.C., Martin, J.M., Wollast, R., Eds.; Wiley: Berlin, Germany, 1991; pp. 69–89.

33. Wiseman, W.J.; Bane, J.M.; Murray, S.P.; Tubman, M.W. Small-scale temperature and salinity structure over the inner shelf west of the Mississippi River delta. *Memo. Soc. Roy. Sci. Liege* **1976**, *6*, 277–285.
34. Lohrenz, S.; Fahnenstiel, G.L.; Redalje, D.G.; Lang, G.A.; Dagg, M.J.; Whittedge, T.E.; Dortch, Q. Nutrients, irradiance and mixing as factors regulating primary production in coastal waters impacted by the Mississippi River plume. *Cont. Shelf Res.* **1999**, *19*, 1113–1141.
35. Dinnel, S.P.; Wiseman, W.J. Fresh-water on the Louisiana and Texas shelf. *Cont. Shelf Res.* **1986**, *6*, 765–784.
36. Rabalais, N.N.; Wiseman, W.J.; Turner, R.E.; Sengupta, B.K.; Dortch, Q. Nutrient changes in the Mississippi River and system responses on the adjacent continental shelf. *Estuar. Coast.* **1996**, *19*, 386–407.
37. D'Sa, E.J. Colored dissolved organic matter in coastal waters influenced by the Atchafalaya River, USA: Effects of an algal bloom. *J. Appl. Remote Sens.* **2008**, doi: 10.1117/1.2838253.
38. Conmy, R.N.; Coble, P.G.; Chen, R.F.; Gardner, G.B. Optical properties of colored dissolved organic matter in the Northern Gulf of Mexico. *Mar. Chem.* **2004**, *89*, 127–144.
39. Shen, Y.; Fichot, C.G.; Benner, R. Floodplain influence on dissolved organic matter composition and export from the Mississippi-Atchafalaya River system to the Gulf of Mexico. *Limnol. Oceanogr.* **2012**, *54*, 1149–1160.
40. D'Sa, E.J.; Dimarco, S.F. Seasonal variability and controls on chromophoric dissolved organic matter in a large river-dominated coastal margin. *Limnol. Oceanogr.* **2009**, *54*, 2233–2242.
41. Schaeffer, B.A.; Conmy, R.N.; Aukamp, J.; Craven, G.; Ferer, E.J. Organic and inorganic matter in Louisiana coastal waters: Vermilion, Atchafalaya, Terrebonne, Barataria, and Mississippi regions. *Mar. Pollut. Bull.* **2011**, *62*, 415–422.
42. D'Sa, E.J.; Steward, R.G.; Vodacek, A.; Blough, N.V.; Phinney, D. Determining optical absorption of colored dissolved organic matter in seawater with a liquid capillary waveguide. *Limnol. Oceanogr.* **1999**, *44*, 1142–1148.
43. D'Sa, E.J.; Steward, R.G. Liquid capillary waveguide application in absorbance spectroscopy. *Limnol. Oceanogr.* **2001**, *46*, 742–745.
44. Osburn, C.L.; St-Jean, G. Stable isotope analysis of dissolved organic carbon in seawater using TOC-IRMS. *Limnol. Oceanogr. Methods* **2007**, *5*, 296–308.
45. Gordon, H.R.; Wang, M. Retrieval of water-leaving radiance and aerosol optical thickness over oceans with SeaWiFS: A preliminary algorithm. *Appl. Opt.* **1994**, *33*, 443–452.
46. Chen, R.F.; Gardner, G.B. High-resolution measurements of chromophoric dissolved organic matter in the Mississippi and Atchafalaya River plume regions. *Mar. Chem.* **2004**, *89*, 103–125.
47. D'Sa, E.J.; Korobkin, M. Colored dissolved organic matter in the northern Gulf of Mexico using ocean color: Seasonal trends in 2005. *Proc. SPIE* **2008**, doi: 10.1117/12.800372.
48. Bianchi, T.S.; DiMarco, S.F.; Smith, R.W.; Schreiner, K.M. A gradient of dissolved organic carbon and lignin from Terrebonne-Timbalier Bay estuary to the Louisiana shelf (USA). *Mar. Chem.* **2009**, *117*, 32–41.
49. Naik, P.; D'Sa, E.J.; Grippo, M.; Condrey, R.; Fleeger, J. Absorption properties of shoal-dominated waters in the Atchafalaya Shelf, Louisiana, USA. *Int. J. Remote Sens.* **2011**, *32*, 4383–4406.

50. Wang, X.C.; Chen, R.F.; Gardner, G.B. Sources and transport of dissolved and particulate organic carbon in the Mississippi River estuary and adjacent coastal waters of the northern Gulf of Mexico. *Mar. Chem.* **2004**, *89*, 241–256.
51. O'Reilly, J.E.; Maritorena, S.; O'Brien, M.C.; Siegel, D.A.; Toole, D.; Menzies, D.; Smith, R.C.; Mueller, M.J.; Mitchell, B.G.; Kahru, M.; *et al.* Ocean Color Chlorophyll-*a* Algorithms for SeaWiFS, OC2, and OC4: Version 4. In *SeaWiFS Post-Launch Calibration and Validation Analyses*; Hooker, S.B., Firestone, E.R., Eds.; NASA Goddard Space Flight Center: Greenbelt, MD, USA, 2000; Volume 11, pp. 9–23.
52. Stramski, D.; Reynolds, R.A.; Babin, M.; Kaczmarek, S.; Lewis, M.R.; Roettgers, R.; Sciandra, A.; Stramska, M.; Twardowski, M.S.; Franz, B.A.; *et al.* Relationships between the surface concentration of particulate organic carbon and optical properties in the eastern South Pacific and eastern Atlantic Oceans. *Biogeosciences* **2008**, *5*, 171–201.
53. Allison, D.B.; Stramski, D.; Mitchell, B.G. Seasonal and interannual variability of particulate organic carbon within the Southern Ocean from satellite ocean color observations. *J. Geophys. Res.* **2010**, doi: 10.1029/2009JC005347.
54. D'Sa, E.J.; Zaitzeff, J.B.; Yentsch, C.S.; Miller, J.L.; Ives, R. Rapid Remote Assessments of Salinity and Ocean Color in Florida Bay. In *The Everglades, Florida Bay, and Coral reefs of the Florida Keys: An Ecosystem Sourcebook*; Porter, J.W., Porter, K.G., Eds.; CRC Press: Boca Raton, FL, USA, 2002; pp. 451–459.
55. Osburn, C.L.; Retamal, L.; Vincent, W.F. Photoreactivity of chromophoric dissolved organic matter transported by the Mackenzie River to the Beaufort Sea. *Mar. Chem.* **2009**, *115*, 10–20.
56. Walker, N.D.; Hammack, A.B. Impacts of winter storms on circulation and sediment transport: Atchafalaya-Vermilion Bay Region, Louisiana, U.S.A. *J. Coastal Res.* **2000**, *16*, 996–1010.
57. Shank, G.C.; Zepp, R.G.; Whitehead, R.F.; Moran, M.A. Variations in the spectral properties of freshwater and estuarine CDOM caused by partitioning onto river and estuarine sediments. *Estuar Coast. Shelf Sci.* **2005**, *65*, 289–301.
58. Corbett, D.R.; Mckee, B.A.; Allison, M.A. Nature of decadal-scale sediment accumulation on the western shelf of the Mississippi River delta. *Cont. Shelf Res.* **2006**, *26*, 2125–2140.
59. Sutula, M.; Bianchi, T.S.; Mckee, B.A. Effect of seasonal sediment storage in the lower Mississippi River on the flux of reactive particulate phosphorus to the Gulf of Mexico. *Limnol. Oceanogr.* **2004**, *49*, 2223–2235.
60. Rouse, L.J.; Coleman, J.M. Circulation observations in the Louisiana Bight using LANDSAT imagery. *Remote Sens. Environ.* **1976**, *5*, 635–642.
61. Walker, N.D.; Wiseman, W.J.; Rouse, L.J.; Babin, A. Effects of river discharge, wind stress, and slope eddies on circulation and the satellite-observed structure of the Mississippi River plume. *J. Coastal Res.* **2005**, *21*, 1228–1244.